TOWARDS MODELLING REGOLITH PERMEABILITY WITH HIGH RESOLUTION X-RAY TOMOGRAPHY

Michael Turner[1], Arthur Sakellariou[2], Christoph Arns[2], Rob Sok[2], Ajay Limaye[3] Tim Senden[2] & Mark Knacktedt[2].

[1]CRC LEME, Department of Applied Mathematics, Research School of Physical Sciences and Engineering, Australian National University, Canberra, ACT, 0200
[2]Department of Applied Mathematics, Research School of Physical Sciences and Engineering, Australian National University, Canberra, ACT, 0200
[3]Vizlab, Supercomputer Facility, Australian National University, Canberra, ACT 0200

INTRODUCTION

The assessment and management of salinity and groundwater contamination issues relating to the distribution, entrainment and behaviour of solutes and contaminants in groundwater and the vadose zone relies upon an understanding of the hydraulic properties of the host regolith. To understand any of the processes governing these issues, an accurate description of the structure characterising hydraulic properties at a scale analogous to the size of the pores is crucial (Webster 1994, Solymar & Fabricius 1999, Kasteel *et al.* 2000), but unfortunately is rarely available (White & Sully 1987, Kasteel, *et al.* 2000, Vogel & Roth 2001, Sok *et al.* 2002).

Distributions of fluid phases within porous materials under unsaturated conditions affects prediction of salt and contaminant dispersion. Moreover, clays, when present, are known to affect flow properties. There is an urgent need to resolve pore-scale information of fluid saturations and clay distributions. This paper describes preliminary work on this subject.

Over the last five years the Department of Applied Mathematics has developed a micro-CT facility capable of acquiring 3D images made up of 2000^3 voxels on core material up to 5cm in diameter with resolutions down to 2 microns. The high brilliance X-ray source (X-Tek) is capable of energies in the range of 30-225 kV and combined with a $(2048)^2$ pixel X-ray camera routinely produces 30 gigabyte datasets. The rotation stage is capable of 0.001 degree steps and has been designed to accommodate a variety of flow and pressure cells. To non-destructively image internal structure, a series of up to 3600 radiographs are collected by rotating the sample incrimentally through 360 degrees. These radiographs are then reconstructed with custom software based on the Feldkamp algorithm (Feldkamp *et al.* 1984) to generate a tomographic data set. Since the ANU facility has a cone beam geometry, the spatial resolution of the tomogram can be set by simply adjusting the distance between the X-ray source and the sample. This allows the 3D pore-space of a rock to be imaged across several orders of magnitude. The collaboration has also developed a suite of software to predict transport (permeability, conductivity, diffusivity) properties directly on digitised tomographic images. Computations of fluid transport properties made directly on the digitised tomographic images have been compared to laboratory core measurements. The results are in excellent agreement (Arns *et al.* 2001, Arns *et al.* 2002, Sok *et al.* 2002).

To extend this work and develop applications crucial to understanding regolith materials, two experimental techniques are being developed:

1. Pore-scale 3D imaging of multiple fluid phases during unsteady state displacement experiments on multiple fluid phase displacements; and,
2. 3D imaging of clay phases and mineralogical differentiation within core material.

The former method is needed when investigating the transport of contaminants in unsaturated materials and the latter is important to understanding the interaction dynamics between the porous material and the pore fluid, especially in the presence of clays. In this paper, we describe preliminary developments of the experimental technique on two model systems: a mono-sized sphere pack; and Berea sandstone.

BEAD PACK

In an attempt to validate the methodology we constructed a model porous media with a known homogenous solid phase—a lightly sintered bead pack with acrylic beads of constant grain size (1.62 ± 0.05 mm). Tomograms were acquired at three stages: dry state; fully saturated with a wetting fluid (vegetable oil); and after the liquid was allowed to drain. The three datasets were co-registered in space and residual fluid was deduced by subtracting the initial dry bead pack from the drained dataset. The resultant residual wetting phase saturation is given in Figure 1.

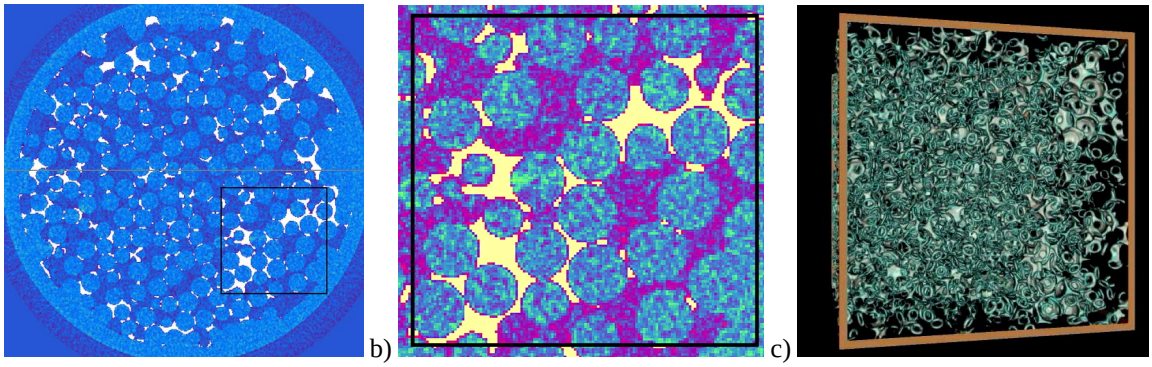

Figure 1: (a) A transverse slice through the 3D dataset of the partially saturated bead pack. The container was a 30 mm diameter acrylic cylinder. (b) Close up of the boxed area in (a). Liquid is yellow. (c) A 3D representation of a portion of the 2D dataset presented in (a). Only the residual oil phase (silver) is visible in this image as the void space and bead volume has been rendered transparent.

From the image it can be seen that, after drainage, the residual wetting phase predominantly resides in the smaller pore restrictions, as expected, and air is predominantly within the larger pore spaces. This phenomenon is more obvious when the 3D image is examined (Figure 1c). Here we observed that disconnected 'pendular rings' account for the bulk of the residual fluid. From the segmented image residual saturation was calculated to be 12% of the total pore space.

BEREA SANDSTONE

Once the experimental procedure was determined for the homogenous bead pack the experiment was repeated on a more complex and realistic system. Berea sandstone, a quartzitic sandstone with an approximately 10% clay fraction, was chosen as it is a petroleum industry standard in rock property experiments and numerous two-phase experiments have been performed on the sandstone (Oak 1991, Øren & Bakke 2003).

The Berea sample was encased in a sleeve of resin producing a no-flow boundary condition. A fluorocarbon wetting fluid replaced the vegetable oil; the wetting properties of fluorocarbon/air mimicked those of previous two-phase flooding experiments (Oak 1991). Tomograms were recorded as for the bead pack: dry; saturated; and drained. Fluid distributions were again deduced by co-registering the image in space and performing image subtraction. Figure 4 shows the distribution of the mineral and 2 fluid phases within the sample after drainage. Figure 4a shows a transverse slice through the dry rock. The phase maps (Figure 4b, c) show a binarised image of the fluid distributions (white: non wetting, and black: wetting) after drainage (grains are grey).

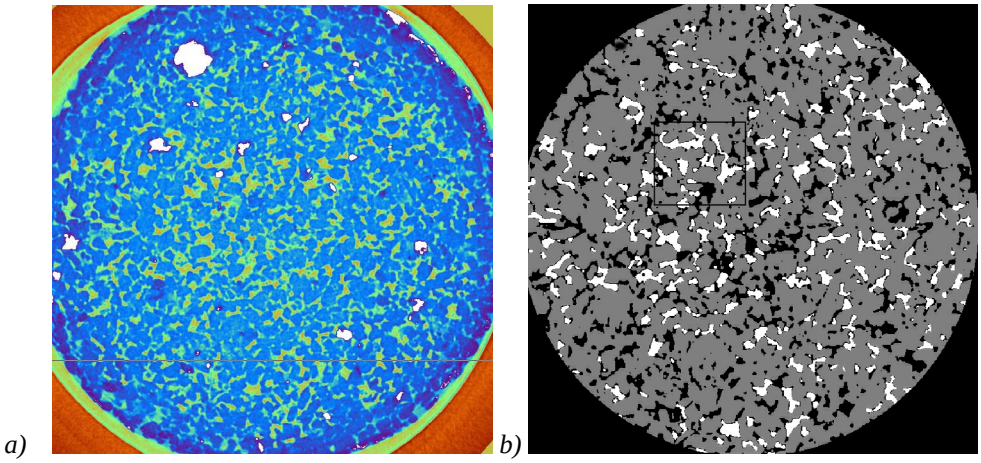

Figure 2: (a) Tomographic slice through the original dry sample prior to segmentation. Blues hues depict solid, orange is pore space, green is an intermediate phase. The sample is ca. 8 mm in diameter. (b) Same slice after segmentation into 3 discrete phases. Liquid is shown in black, air is white and the substrate is grey.

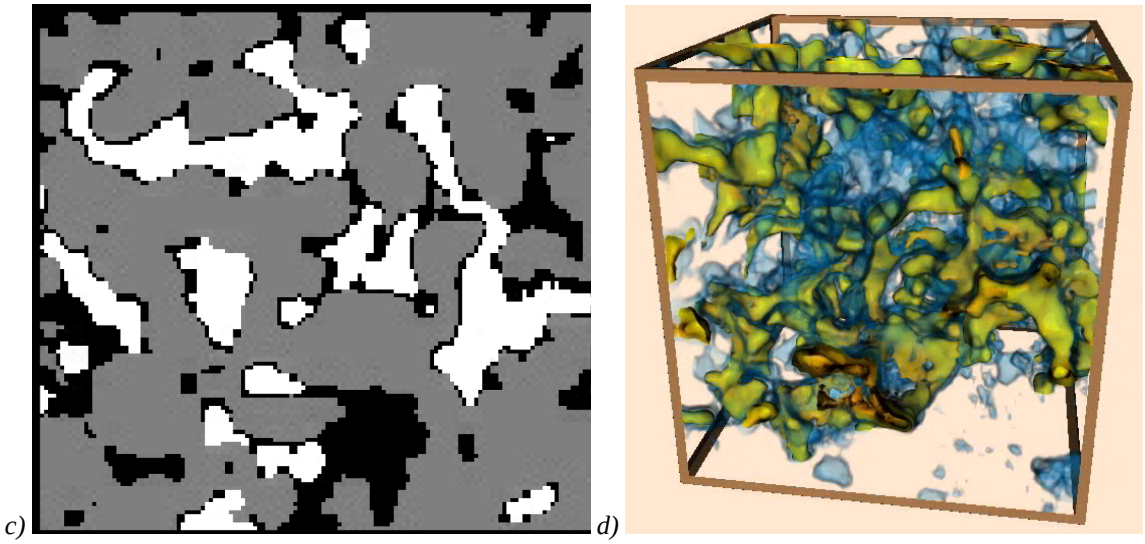

c) *d)*

Figure 3 (continued): (c) Enlargement of (b). (d) a 3D rendering of a portion (ca. 1 mm^3) of the initial dataset showing all three phases and their relative distribution. The solid mineral phase is transparent in this image with pore space in green and residual fluid in blue.

The pores in Berea sandstone are irregularly shaped and in most cases larger pores are joined by much smaller and narrower throats. As in Figure 1, it can again be seen that the residual fluid phase after drainage predominantly resides in the smaller pore restrictions and the air-filled void is predominantly within the larger pore spaces. We also note that many air filled pores (Figure 4c) have films of wetting phase within them. A 3D image is given in Figure 4d.

CLAY DISTRIBUTION

In most samples the X-ray attenuation of clay lies intermediate to the predominant mineral phase grains and open pore space, and unfortunately cannot be directly distinguished from a tomogram. Berea sandstone has a large clay fraction of approximately 10% (Øren & Bakke 2003). Here we described a technique to enhance the contrast of the clay phase within Berea sandstone. Preliminary data is presented.

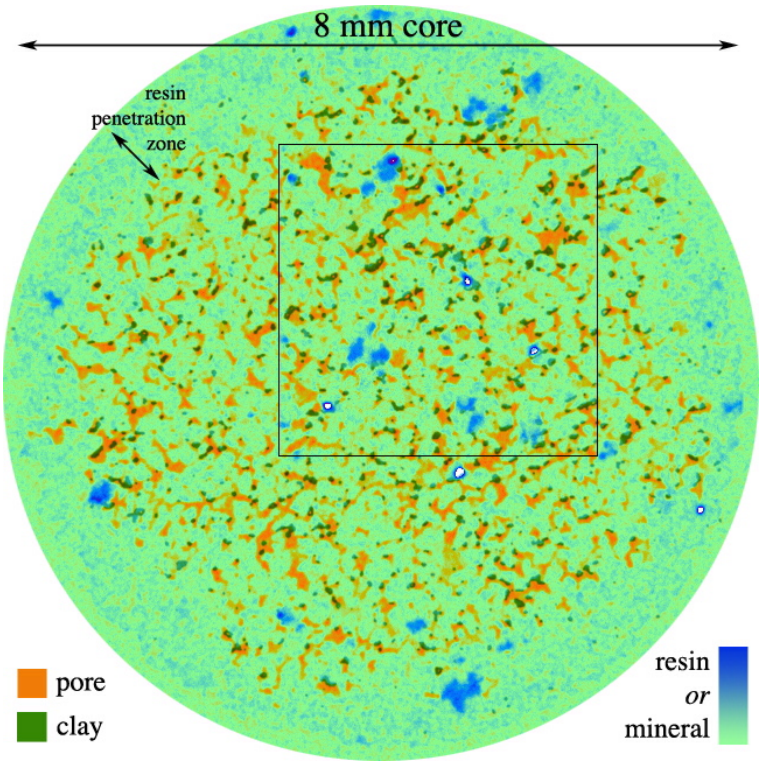

Figure 4: The raw dataset with the clay overlay in dark green.

Again, three tomograms were collected. The first when the sample was in a dry native state (Figure 5a). The second when the sample was saturated with a 0.07M CsBr solution, and the third after the CsBr solution had been flushed out with ethanol. CsBr was chosen for its high X-ray attenuation and the ability of the Cs cations to exchange with any clay-bound cations, thereby increasing the relative X-ray attenuation within the clay phase. By subtracting the dry image from the ion exchanged sample a difference map was generated and was overlayed on the original data to delineate the clay rich areas (Figure 3). Comparing the dry sample (Figure 5a) with the labelled sample (Figure 5b), it can be seen that areas designated clay (darker green) almost always occur in areas designated pore. The volume fraction of clays measured in the sample was 11%; this is consistent

with results obtained in other studies. Øren & Bakke (2003) report that of the 9% volume fraction of authigenic clay in a Berea sample, some 90% was pore-filling and the rest pore-lining. It can be seen from Figure 5b that most of the area labelled clay fraction in this work occurs as pore-filling.

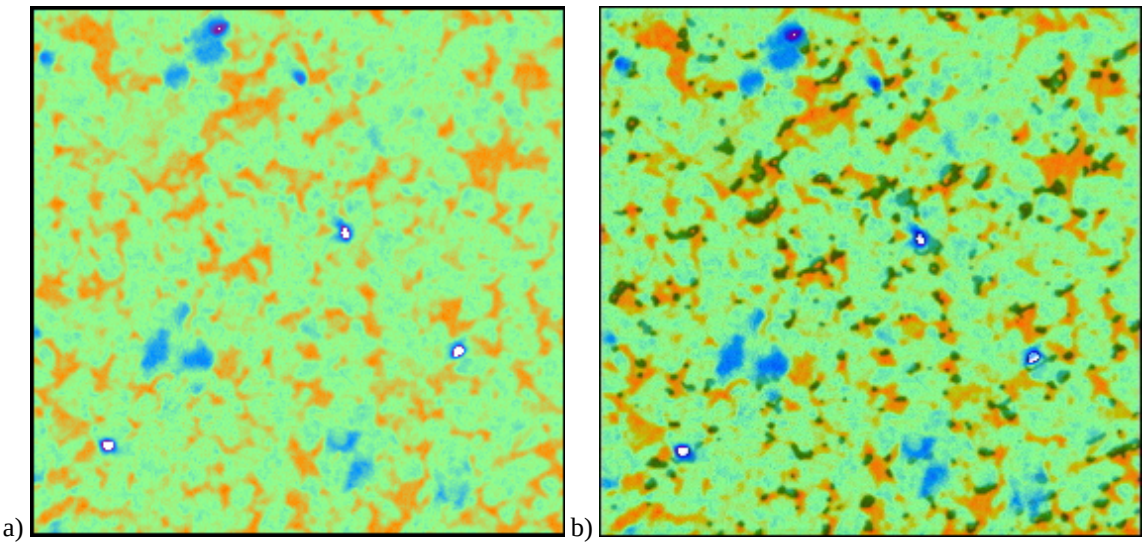

Figure 5: A portion (4 mm^2) of an 8 mm Berea core. (a) The raw data of the Berea core in a dry state. Green and blue is granular substrate, orange is pore space. (b) Same as (a), but with an overlay of the difference map between the dry substrate and the Cs-exchanged clays.

The spatial distribution of clays is of great importance to the understanding of fluid flow in regolith materials. Surprisingly, we found that the labelled phase did not always coincide with those areas that appeared to possess intermediate attenuation properties. Although this procedure shows promise, parallel SEM studies on sections from the sample are required to prove the technique; this work is ongoing.

CONCLUSIONS

An understanding of the processes governing groundwater contamination and remediation or the entrainment and behaviour of solute and contaminants in the saturated and vadose zones requires an accurate description of the structure at the pore-scale. The prediction of flow properties is ultimately dependent on details from the pore structure. In this investigation preliminary development and validation of several novel experimental techniques for measuring important pore-scale information of reservoir rocks has been completed. Extensions to regolith materials should be straightforward. The utility of the ANU micro-X-ray facility in resolving the spatial distribution of the fluid and mineral phases in one idealised and one complex porous media has been shown.

The longer-term goal of this work will involve a study of well-characterised regolith samples provided by the Bureau of Rural Science from a site near St. George, Queensland, in an attempt to characterise their hydraulic properties and mineral distributions. In this application a number of techniques remain to be developed, and questions remain to be answered. These include:

- the development of a technique to reliably subsample friable regolith materials;
- collection of time-series data that covers the entire length of the experimental period and includes partial saturation time steps;
- further verification of labelling methods for delineating a clay phase;
- the effect differing electrolyte concentrations have upon different combinations of mineral and morphology found in regolith materials;
- tracking flow to identify contaminant transport properties; and,
- up-scaling of the data for use in field-scale applications that can use the information obtained through this type of investigation to develop predictive models.

REFERENCES

ARNS C.H., KNACKSTEDT M.A., PINCZEWSKI W.V. & LINDQUIST W.B. 2001. Accurate estimation of transport properties from microtomographic images. *Geophysical Research Letters* **28(17)**, 3361-3364.

ARNS C.H., KNACKSTEDT M.A., PINCZEWSKI W.V. & GARBOCZI E.J. 2002. Computation of linear elastic properties from microtomographic images: Methodology and agreement between theory and experiment. *Geophysics* **67(5)**, 1396-1405.

FELDKAMP L.A., DAVIS L.C. & KRESS J.W. 1984. Practical Cone-Beam Algorithm. *Journal of the Optical Society of America A - Optics Image Science and Vision* **1(6)**, 612-619.

KASTEEL R., VOGEL H.-J. & ROTH K. 2000. From local hydraulic properties to effective transport in soil. *European Journal of Soil Science* **51**, 81-91.

OAK M.J. 1991. Three-Phase Relative Permeability of Intermediate-Wet Berea Sandstone. *In: 66th Annual Technical Conference and Exhibition of the Society of Petroleum Engineers*. Society of Petroleum Engineers, Richardson, Texas.

ØREN P.E. & BAKKE S. 2003. Reconstruction of Berea sandstone and pore-scale modelling of wettability effects. *Journal of Petroleum Science and Engineering* **39**, 177-199.

SOK R.M., KNACKSTEDT M.A., SHEPPARD A.P., PINCZEWSKI W.V., LINDQUIST W.B., VENKATARANGAN A. & PATERSON L. 2002. Direct and stochastic generation of network models from tomographic images; Effect of topology on two phase flow properties. *Transport in Porous Media* **46**, 345-372.

SOLYMAR M. & FABRICIUS I.L. 1999. Image Analysis and Estimation of Porosity and Permeability of Arnager Greensand, Upper Cretaceous, Denmark. *Physics and Chemistry of the Earth (A)* **24(7)**, 587-591.

VOGEL H.-J. & ROTH K. 2001. Quantitative morphology and network representation of soil pore structure. *Advances in Water Resources* **24**, 233-242.

WEBSTER R. 1994. The development of pedometrics. *Geoderma* **62**, 1-15.

WHITE I. & SULLY M.J. 1987. Macroscopic and microscopic capillary length and time scales from field infiltration. *Water Resources Research* **23(8)**, 1514-1522.